Geomechanics and Engineering, *Vol. 43, No. 5 (2025) 405-417*
https://doi.org/10.12989/gae.2025.43.5.405

Investigating the influence of compressive strength on energy release and instability mechanisms of modeled rock-like models containing prefabricated fissures based on AE and DIC technology

Xianxiu Lu[1], Zhandong Su*[1,2], Zeqi Hao[1], Jianyong Zhang[1,2], Xiaoli Liu[3], Mingdong Zang[4], Jinzhong Sun[4] and Wenqiang Chi[5]

[1]*School of Disaster Prevention and Reduction Engineering, Institute of Disaster Prevention, Langfang, China, 065201*
[2]*Key Laboratory of Earthquake Disaster Prevention and Risk Evaluation of Hebei Province, Langfang, China, 065201*
[3]*State Key Laboratory of Hydroscience and Engineering, Tsinghua University, Beijing, China, 100084*
[4]*College of Engineering and Technology, China University of Geosciences, Beijing, China, 100083*
[5]*China Railway 24th Bureau Group Zhejiang Engineering CO., LTD. Zhejiang, China, 310001*

(*Received November 27, 2024, Revised November 15, 2025, Accepted December 4, 2025*)

Abstract. Rock fracture is a process of energy accumulation and subsequent release, in which rock mass strength significantly influences this process. This study investigates the energy release and evolution of failure mechanisms in models with different compressive strengths through uniaxial compression tests, acoustic emission techniques, and digital image correlation. The experimental results indicate that during the yielding stage, there is a notable increase in the number of small-scale failures in the models. The failure of the models, initially dominated by shear failure, progressively involves more tensile cracks. Before global instability occurs, significant horizontal relative displacement and localized surface deformation are observed at the pre-existing fissures. As the strength decreases, the models tend to exhibit a larger number of small-scale failures, and the failure mechanism shifts toward a composite shear-tensile mode.

Keywords: energy; failure mechanism; local deformation; rock-like model

1. Introduction

The stability of rock mass engineering is predominantly governed by the initiation, propagation, and coalescence of internal fractures. These processes are inherently energy-driven: external loads perform work on the rock mass, leading to the storage and transformation of energy within it, which is ultimately dissipated and released through fracture. The fracture mechanism of rock—whether tensile, shear, or a composite of both—is an external manifestation and inevitable outcome of specific energy evolution pathways. A profound understanding of how material strength influences this process is crucial for fundamentally comprehending the precursors and evolutionary laws of rock mass instability.

Natural rock masses contain numerous structural discontinuities—such as pores, joints, and bedding planes—with irregular geometries and random spatial distributions (Zhang *et al.* 2024, Cheng *et al.* 2024, Yu *et al.* 2022). These discontinuities dominate the macroscopic mechanical behavior and failure modes of rock masses. In underground engineering projects like tunneling, excavation-induced unloading causes stress redistribution within the rock mass system, driving the propagation of pre-existing fractures and the initiation of new ones (Ratan *et al.* 2021, Farhadian *et al.* 2025, Cai *et al.* 2022, Zhu *et al.* 2023). When external loads act on the rock mass, significant local deformation occurs at fracture tips, forming the so-called "Fracture Process Zone" (Zhang *et al.* 2020).

Field fault zones can be divided into creeping segments with noticeable surface deformation and locked segments that accumulate energy (Su *et al.* 2021, Guo *et al.* 2025, Mostafa and Manoochehr 2018), Earthquakes occur when the locked segments release energy. These local damage events act as precursors to energy release, providing a physical basis for predicting macroscopic failure. It is noteworthy that even under similar geological conditions, the energy release processes and instability mechanisms vary across different types of rocks (Zhou and Zhang 2021, Zhou *et al.* 2022, Aligholi *et al.* 2024, Liu *et al.* 2021). Although existing research has yielded substantial results regarding the evolution of pre-existing fractures, and the stability of engineering rock masses, the regulatory mechanism of material strength on local fracture deformation behavior and the global failure process still requires further exploration. With advancements in digital image correlation (DIC) technology, researchers can now perform full-field deformation measurements on rock surfaces and accurately track crack propagation processes (Wu *et al.* 2021). Numerous studies have shown that different failure modes, such as tensile and shear, are closely related to energy conversion paths and local stress states. Understanding this relationship is crucial for predicting global instability through local damage signals.

*Corresponding author, Professor
E-mail: szdchris@163.com

Copyright © 2025 Techno-Press, Ltd.

ISSN: 2005-307X (Print), 2092-6219 (Online)

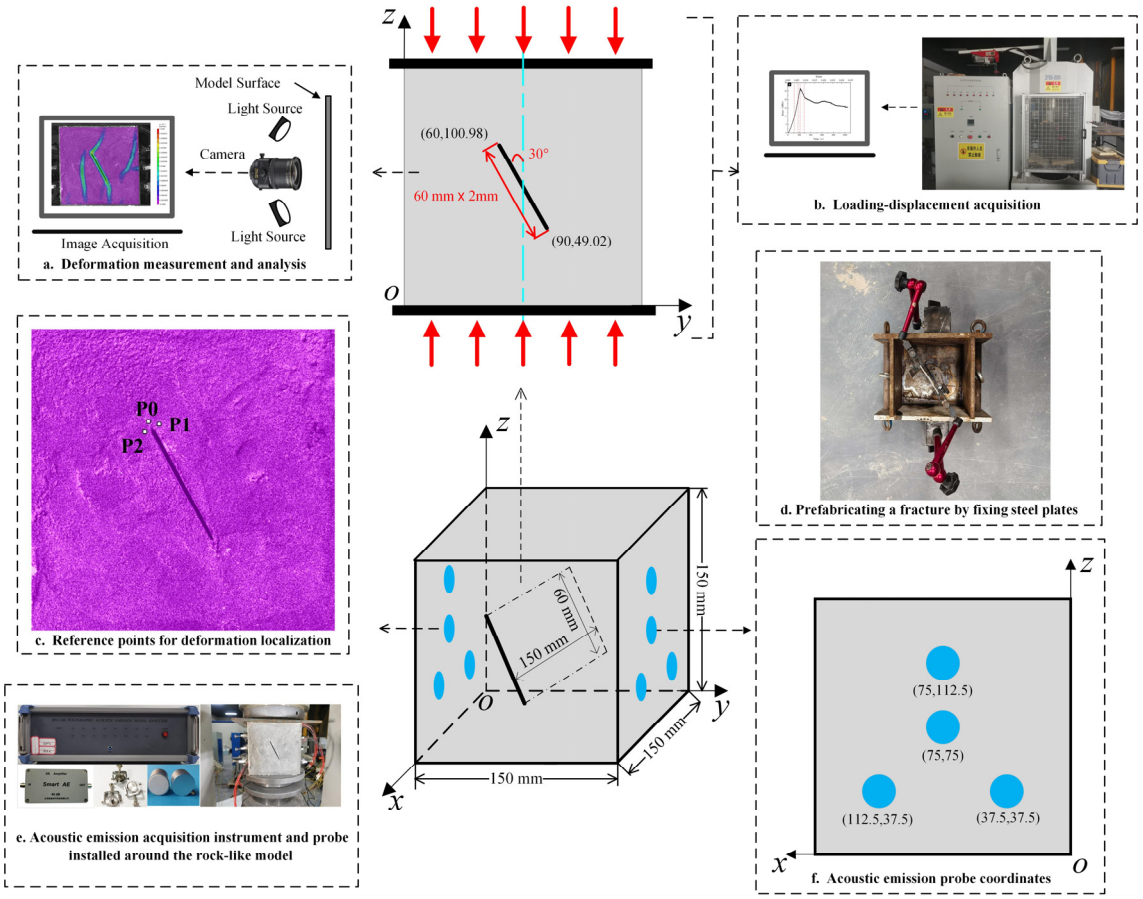

Fig. 1 Schematic diagram of the rock analog model experiment. The coordinates represent the centroid of acoustic emission monitoring points and the endpoints of the prefabricated fissure. The coordinates are the detection point coordinates for the acoustic emission and endpoint coordinates for the prefabricated fissure

Acoustic emission technology offers an effective means to monitor this process, allowing for the inversion of internal micro-fracture evolution laws and identification of fracture mechanisms. Currently, the combined application of digital image correlation technology and acoustic emission technology has become a research focus. For example, Niu *et al.* (2023a) studied the characteristics and damage of filler materials in fractured rocks. Miao *et al.* (2021) investigated the cracking process of rocks under static and minor dynamic disturbances. Other scholars have used the RA-AF value of acoustic emission parameters to quantitatively analyze the proportion of shear to tensile cracks during rock failure (Chen *et al.* 2024b, Du *et al.* 2024, Li *et al.* 2022). These experiments confirm that rock failure is a gradual process from internal micro-damage accumulation to external macro-fracture (Wang *et al.* 2021, Dong *et al.* 2022). However, natural rock samples inevitably undergo stress disturbances during sampling, and their failure modes are significantly influenced by the distribution of original micro-fractures (Manouchehrian *et al.* 2014, Rezvan *et al.* 2023). Therefore, some scholars have utilized rock analog materials to create models for optimizing research subjects (Zhang *et al.* 2015, Zuo *et al.* 2007, Cui *et al.* 2023, Haeri *et al.* 2014a, Haeri *et al.* 2014b). The mechanical properties of these models can be tailored by adjusting mix proportions and types of admixtures (Niu *et al.* 2023b). These materials not only ensure the homogeneity and repeatability of the internal structure of specimens but also provide an ideal medium for systematic parametric studies. Nevertheless, systematic research on how material strength affects damage evolution, energy distribution, and fracture mechanisms is still relatively lacking. In particular, the strain localization phenomenon, where fracture zone deformation precedes global deformation, still needs to be quantitatively correlated with material strength.

Based on this, this study designed four types of rock-like material mixes with different uniaxial compressive strengths. Using a combination of acoustic emission and digital image correlation techniques, it systematically investigates the influence of material strength on local deformation behavior at fracture tips, energy evolution laws, the transition of fracture mechanisms, and the global failure process.

2. Materials and methods

In this experiment, the model strength was regulated by adjusting the aggregate content and the proportions of

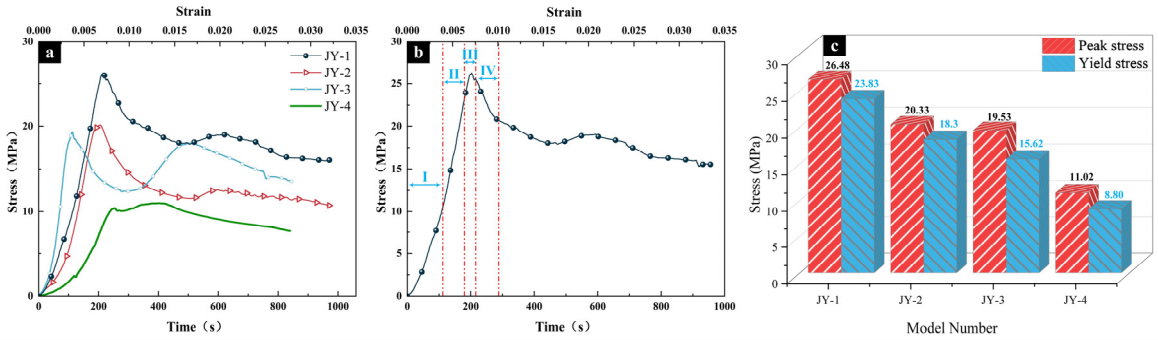

Fig. 2 Mechanical properties of the model: (a) Stress-strain curve, (b) Schematic division of different failure stages and (c) Peak strength and yield strength

Table 1 Ratio of sample preparation materials

Model number	Aggregat/ Cementing material	Barite/ Aggregate (%)	Sand (g)	Barite (g)	Gypsum (g)	Water (g)	Compressive strength (MPa)	Elastic modulus (GPa)
JY-1	2:1	10	600.0	66.6	333.3	250.0	26.48	5.05
JY-2	3:1	15	637.5	112.5	250.0	250.0	20.33	5.11
JY-3	4:1	20	640.0	160.0	200.0	250.0	19.53	8.22
JY-4	5:1	25	625.0	208.3	166.6	250.0	11.02	2.14

aggregate components. The quantities of each material component are listed in Table 1. The VIC-2D photography and analysis system was employed to examine surface deformation of the models, while an acoustic emission acquisition system was used to collect internal cracking characteristics and analyze the corresponding failure mechanisms. Specific parameters can be referenced from previous studies(Su *et al.* 2025a, Wang *et al.* 2025). Fig. 1 illustrates the experimental procedure.

The rock models were cubic in shape, with prefabricated fissures created using steel plates. The fracture dimensions were 60 mm in length × 2 mm in width. After preparation, the models were left undisturbed for 24 hours before demolding, followed by curing under laboratory conditions (25°C; humidity: 50%) for 3 days. Prior to testing, the front surface of the models was sprayed with black paint dots. Acoustic emission sensors were also attached to both left and right sides of the models in an array pattern as shown in Fig. 1(f). A uniaxial compression experiment was performed at a uniaxial loading rate of 0.005 mm/s, the shooting frequency of the high-speed camera is 2 frames per second.

3. Experimental results

The stress-strain characteristics of the model can be divided into the pore compaction stage (I), elastic stage (II, conforming to Hooke's law), yield stage (III), and post-peak stress stage (IV). This experiment concluded observations in the post-peak stage when visually identifiable cracks appeared on the surface. Based on the characteristics of the stress-strain curve and the corresponding experimental data, the time nodes of each failure stage are determined (Fig. 2(b)), and the yield strength of the four models exhibits a significant gradient variation (Fig. 2(c)). Table 2 presents the distribution of the corresponding time periods.

Table 2 Time points corresponding to the reference line (s) of each stage

Stage	JY-1	JY-2	JY-3	JY-4
I	112	91	48	141
II	182	173	92	216
III	216	207	111	249
IV	288	251	173	287

3.1 Damage evolution process of rock-like models

3.1.1 Analysis of the model's energy evolution process

Rock failure is typically caused by the accumulation, dissipation, and release of energy (Wang *et al.* 2024a, Wang *et al.* 2023, Wang *et al.* 2024b). First, an analysis is conducted at the overall level of the rock-like mass to explore the energy evolution characteristics of the entire rock-like specimen during uniaxial compression.

Assuming that the rock-like specimen behaves as a closed system during uniaxial compression, the energy equation based on the first law of thermodynamics is as follows (Zhang *et al.* 2025b)

$$U = U^{\mathrm{e}} + U^{\mathrm{d}} \tag{1}$$

where: U is the total input energy; U^e is the stored elastic strain energy; U^d is the dissipated strain energy.

In uniaxial compression experiments, the total energy absorbed by the rock-like mass is

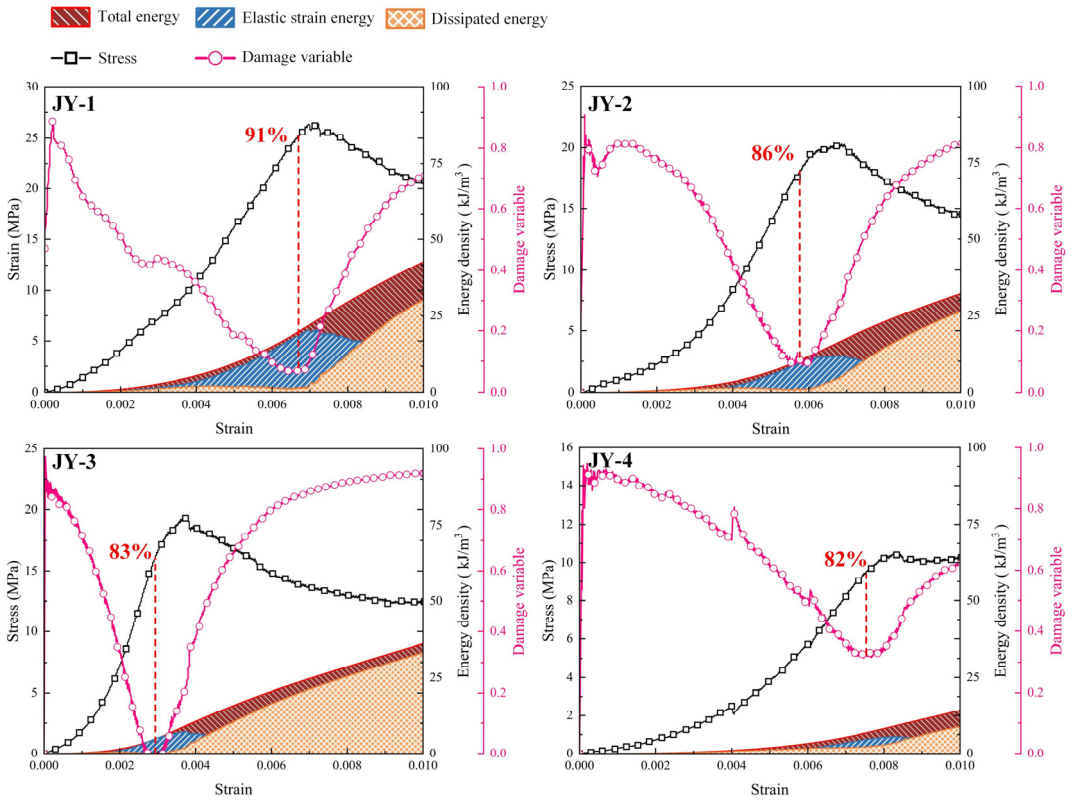

Fig. 3 Energy release characteristics of the rock-like model, expressed as a percentage of the stress level relative to the peak stress

$$U = \int \sigma_1 d\varepsilon_1 = \sum_{i=1}^{n} \frac{1}{2}(\varepsilon_{1,\ i+1} - \varepsilon_1)(\sigma_{1,\ i+1} + \sigma_1) \tag{2}$$

where: σ_1 is the stress; ε_1 is the strain.

The elastic strain energy can be expressed as

$$U^e = \frac{1}{2}\sigma_1 \varepsilon_1^e = \frac{\sigma_1^2}{2E_u} \approx \frac{\sigma_1^2}{2E_0} \tag{3}$$

E_0 is the initial elastic modulus.
Thus, the dissipated strain energy is

$$U^d = U - U^e \tag{4}$$

The damage variable is defined as follows

$$D = \frac{U_d}{U} \tag{5}$$

Using the above formulas and experimental data, the energy release curves and peak energy values of the rock-like model are obtained, which are then analyzed in conjunction with the stress-strain-time curves (Fig. 3).

Fig. 3 illustrates that before general yielding occurs, the input energy in rock-like specimens is predominantly stored as elastic strain energy, with a marked drop in the dissipated energy share. After yielding, energy dissipation increases rapidly, and the elastic energy proportion declines accordingly. In this stage, nearly all input energy is released through dissipation, eventually causing surface cracking post-peak

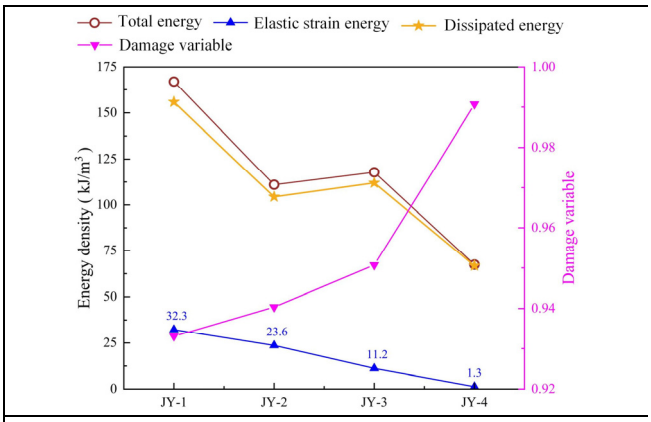

Fig. 4 Comparison of energy parameters of the models

stress. Notably, comparative analysis indicates that the stress level (as a percentage of peak stress) corresponding to the transition point where the damage variable (represented by the dissipated energy ratio) begins to rise decreases with lower material strength.

By integrating the maximum total energy, maximum elastic strain energy, maximum dissipated energy, and the maximum proportion of dissipated energy for all four specimen types, the results are presented in Fig. 4.

Based on the foregoing analysis, during rock failure, dissipated energy can be divided into two components: energy consumed by internal friction and energy expended in rock fracturing. Thus, the primary driving force behind rock rupture originates from dissipated energy. The generation of new

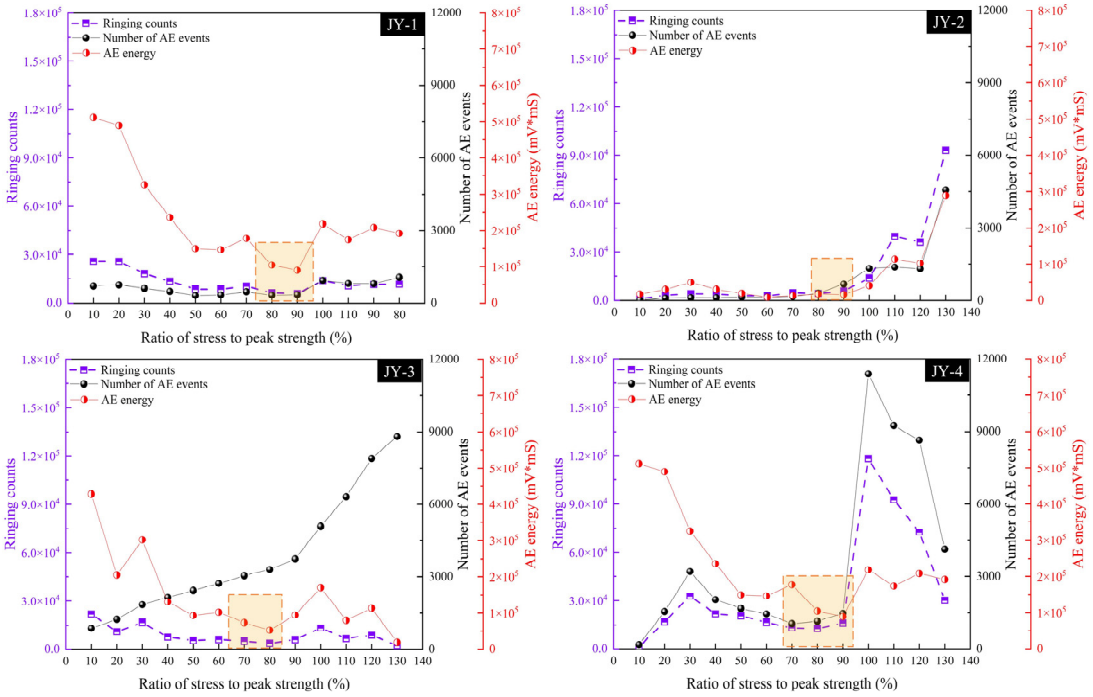

Fig. 5 Acoustic emission characteristics of the rock-like models

cracks in rock materials requires energy dissipation, as does slip along existing fracture surfaces. Consequently, the yielding failure and damage-induced fracture of rock materials are essentially processes of energy dissipation. Upon rock mass rupture, elastic energy is rapidly released. A sharp decrease in elastic energy at its peak, a sudden and rapid rise in dissipated energy, and an increase in the ratio of dissipated energy to total input energy can serve as indicators of fracture closure and the initiation of surface cracking in fractured rock-like masses. Furthermore, the point at which the growth rate of the damage variable stabilizes can be regarded as the starting point of the second peak in fractured rock-like masses, also signifying the completion of surface crack development.

3.1.2 Differences in the number of ruptures in models

AE ring-down count and AE energy are commonly used to reflect internal fracturing within the model(Miao *et al*. 2024, Xu *et al*. 2022). As shown in Fig. 5, the variation trends of AE ring-down counts and AE energy exhibit good correlation, with both showing a significant increase before the peak stress. It is worth noting that for model JY-3, AE events continue to increase substantially after the peak stress, while the AE energy shows a declining trend. This indicates a tendency toward a large number of low-energy ruptures. In the case of model JY-4, a large number of AE events occur in the stage from 90% to peak stress, yet the increase in AE energy is relatively insignificant, suggesting that the fractures are also numerous but low in energy. The number of AE events only reflects the total count of acoustic emissions, whereas AE ring-down counts and AE energy are more responsive to signal intensity and frequency. During the 80% to 100% peak stress level stage, these models enter a brief trough in AE ring-down counts, AE event counts, and AE energy, indicating fewer fractures at this time. This stage generally corresponds to the elastic stage in Fig. 3, where the models are in a state of energy accumulation. Overall, the AE ring-down counts and AE energy of the four models show a trend of high–low–high, and this trend becomes more pronounced with decreasing strength.

3.1.3 Differences in AE energy of models

To reflect the development of the model damage level during compression, the AE energy versus time curves for the four models are plotted against the model stress versus time curves, as shown in Fig. 6.

The acoustic emission (AE) energy of the four models exhibited a transition from low to high levels before gradually decreasing to lower levels. The peak in AE energy generally occurred during the elastic stage, followed by a rapid return to low levels in the third stage. Among them, the JY-1 model showed concentrated release of AE energy, while the other models exhibited relatively uniform energy release with more frequent and sustained ruptures.

There was a clear sequential relationship between the characteristics of AE energy release and the overall energy release process of the models. For models JY-1 to JY-3, significant energy dissipation was observed after the AE energy peak. The AE signals indicated that as the strength decreased, post-peak stress behavior tended toward small-scale failures.

The substantial release of AE energy suggests that the rupture energy release in the models was primarily concentrated near the peak stress. As shown in Fig. 5, the process from 30% to 80% of the peak stress was mainly characterized by the continuous propagation and interconnection of small-scale ruptures, during which energy accumulated within the models (Fig. 3). Before

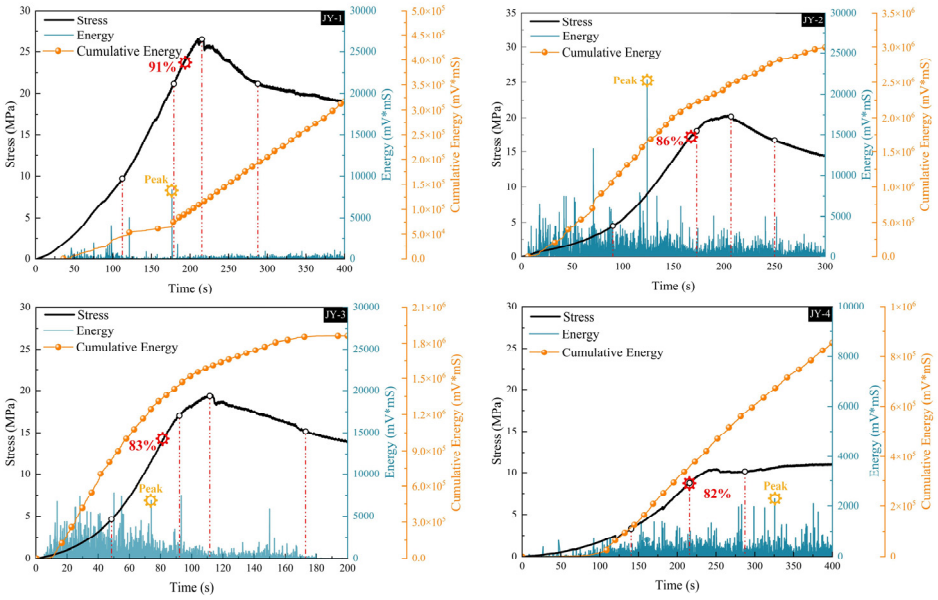

Fig. 6 Acoustic emission energy characteristics of rock-like models

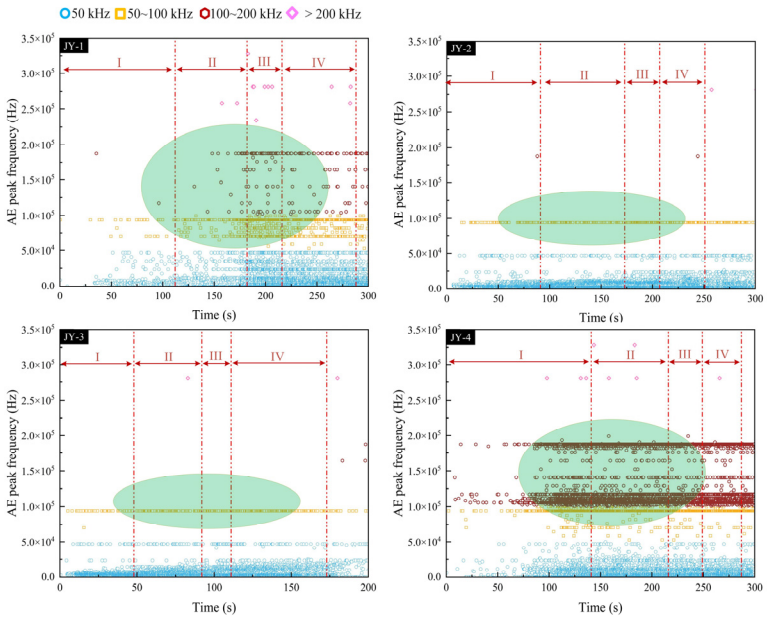

Fig. 7 Peak frequency of acoustic emission signals

entering the yielding stage, a short-term large energy release occurred, promoting further connection and penetration of microcracks. Subsequently, the models tended to undergo numerous small-scale ruptures, with the accumulated energy being continuously released, ultimately driving the formation of a macroscopic rupture surface.

Regarding the variability in rupture scale, this can also be correlated with the distribution characteristics of the AE peak frequency (Li *et al*. 2024a). Fig. 7 illustrates the distribution of the AE peak frequency during the loading process of the rock-like models.

The peak frequencies of each model exhibit a banded distribution, which can be categorized into four frequency ranges. Low-frequency signals (below 50 kHz) correspond to large-scale fractures, while medium- and high-frequency signals (50–200 kHz) correspond to small-scale fractures. Low-frequency signals are widely distributed across all four models. However, it is noteworthy that from the beginning of Stage II until the peak stress is reached, the number of medium- and high-frequency signals in the models significantly increases (as indicated by the shaded area in the graph). This suggests that as the models begin to yield overall, the process is primarily driven by small-scale fractures connecting and penetrating existing cracks, ultimately forming a macro-fracture plane (Wu *et al*. 2025). The JY-4 model even exhibits fracture characteristics dominated by medium- and high-frequency signals, indicating that small-scale fractures play a predominant role in its damage process.

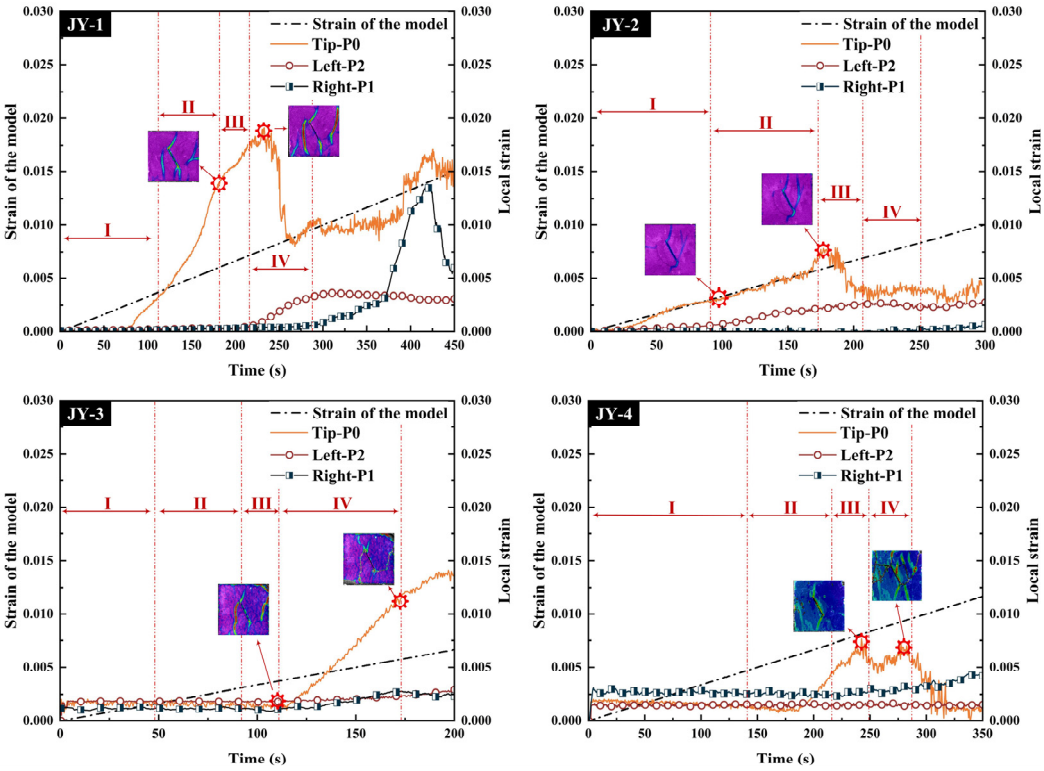

Fig. 8 Comparison of the local strain at the tip of the prefabricated fissure with the strain of the model

Low-strength models are more prone to generating a large number of low-energy, small-scale fractures(Yang *et al.*, 2024), whereas high-strength models tend to produce large-scale events characterized by high energy and low frequency (as shown in Figs. 5 and 6). This can be attributed to the enhanced suppression of micro-fractures by the material strength around the prefabricated fissures.

3.2 Modeled destabilization evolution

3.2.1 Evolution of local strain

The region where significant deformation first occurs at the tip of a prefabricated fissure due to stress concentration is termed the fracture process zone. The rapid development of this zone constitutes a critical stage in the model's damage progression (Wu *et al.* 2022). This study established three monitoring points on the model surface (Fig. 1(c)) to observe local deformations.

As shown in Fig. 8, prior to the overall instability of the model, there is a distinct phase where local deformation grows significantly faster than the global deformation. Models with higher compressive strengths exhibit greater magnitude of local deformation during this phase and can withstand larger local strain. Before surface cracking occurred in the four models, the maximum differences between local strain and global strain were 0.019, 0.014, 0.006, and 0.005, respectively.

Following the peak stress phase, the local deformation rate of the specimen significantly surpasses the overall deformation rate. The development of deformation in the plastic zone exerts a restraining effect on the continued deformation of the tension zone. It is particularly noteworthy that although specimens JY-2 and JY-3 exhibit similar strength parameters, the higher elastic modulus of JY-3 delays the onset of accelerated local deformation. However, the impact of local damage on global stability is more pronounced in JY-3, confirming that material stiffness significantly influences crack propagation behavior. Under displacement-controlled loading conditions, specimens with higher elastic modulus demonstrate faster stress accumulation and more notable stress concentration at defect sites. This characteristic provides greater energy accumulation for local deformation, ultimately promoting the rapid development of brittle failure modes. It is this brittle nature that causes JY-2 to undergo sudden failure before significant local deformation occurs (Fig. 8). During the III stage, the emergence of numerous micro-scale fracture signals effectively slows the growth rate of local strain, revealing the intrinsic relationship between surface strain state and internal fracture dimensions. While macroscopic fractures trigger significant development of surface deformation, this growth becomes noticeably constrained as the specimen approaches the critical point of global instability.

Meanwhile, by comparing the strain levels on both sides of the prefabricated fissure, it can be observed that the left side of the model, being closer to the active loading end (with the press applying pressure from the lower end), exhibits more pronounced deformation. This is manifested as a clear trend of upward movement in the left-side material and downward movement in the right-side material. This trend becomes less evident as the material strength decreases, indicating that the overall deformation of the model can accommodate localized deformation. To verify the relative slip between materials on both sides of the model, the horizontal component was utilized to refine the analysis of the full-field deformation process.

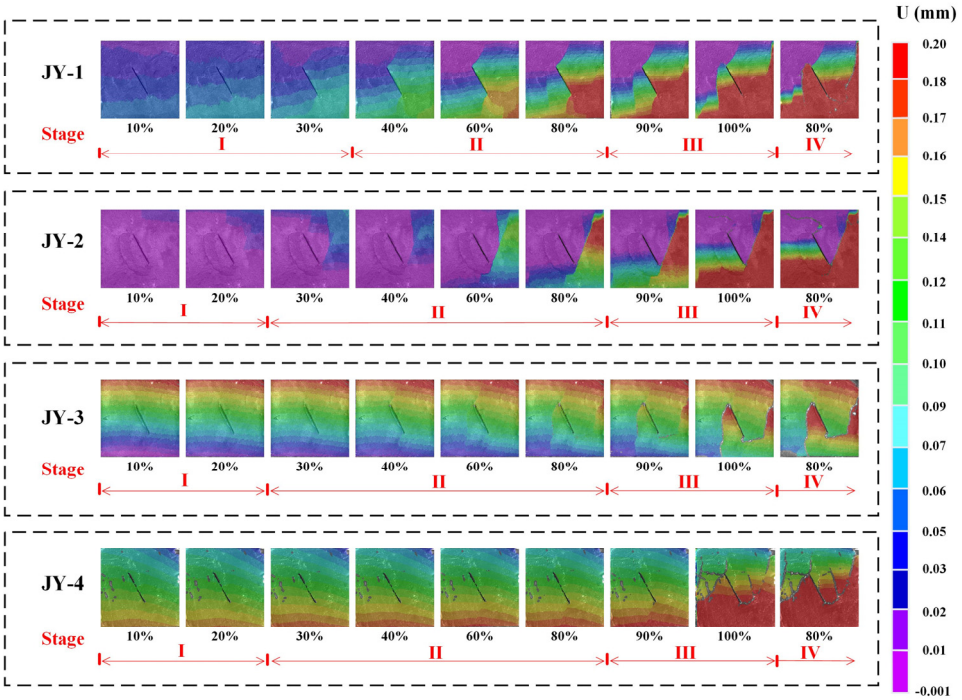

Fig. 9 Surface deformation of the models corresponding to different deformation stages and stress levels. The percentage is the ratio of the stress applied to the model to the peak stress. U: Horizontal displacement component

3.2.2 Full-field deformation evolution on the model surface

The surface deformations of the model under different stress levels are illustrated in Fig. 9. Prior to the penetration of the fracture surface, the materials on both sides of the prefabricated fissure exhibit noticeable horizontal slip components, demonstrating distinct shear failure characteristics. This indicates that the presence of the prefabricated fissure significantly influences the failure mechanism of the model(Meng *et al*. 2025). Furthermore, it is observed that as the strength decreases, the stress percentage at which this significant slip occurs increases. This suggests that the models possess a certain capacity to accommodate deformation in response to external stress, with lower-strength models exhibiting a greater ability for such accommodation. This is manifested as a longer compaction phase and a larger overall strain in the model (e.g., JY-4). Compared to the JY-2 model, the JY-3 model has a lower yield strength and a higher elastic modulus, resulting in a relatively more rapid and less detectable rupture evolution process (Chen *et al*. 2024a, Cui *et al*. 2023).

4. Discussion

To gain deeper insights into the influence of compressive strength on the energy release characteristics and fracture mechanisms of cracked rock-like models, acoustic emission technology and DIC technology were employed to monitor both internal and external damage evolution. Further discussion and summary will be presented in two sections.

4.1 Internal damage characteristics of rock-like models

The overall failure of the model manifests as a phased and progressive process. With increasing load, it can be further divided into an energy accumulation stage and a rapid release stage (Fig. 3). Prior to reaching the peak stress, a noticeable decline in ring-down count and acoustic emission energy is observed (Fig. 5). From the yield stage until after the peak stress, the model releases substantial energy. Models with lower compressive strength exhibit poorer energy storage capacity and tend to generate numerous low-energy signals, resulting in relatively dispersed energy release. This large-scale damage signal primarily concentrates near the peak stress (approximately 90% of the peak value), where both the acoustic emission ring-down count and energy show a significant increase.

The fracture scale of the model underwent a transition from large-scale to small-scale and back to large-scale (Figs. 5 and 7). Notably, during the yield stage, the number of small-scale fractures increased, while the growth rate of both local strain and overall stress decelerated. The surface deformation of the model exhibited three distinct phases: accelerated increase, slow increase, and accelerated decrease (Fig. 8). These processes were temporally synchronized.

4.2 Evolution of fracture mechanisms

The fracture mechanisms of the model can be determined using RA-AF values, with the corresponding diagram plotted as shown in Fig. 10. (Chen *et al*. 2024b, Du *et al*. 2024, Hu Bailin *et al*. 2025).

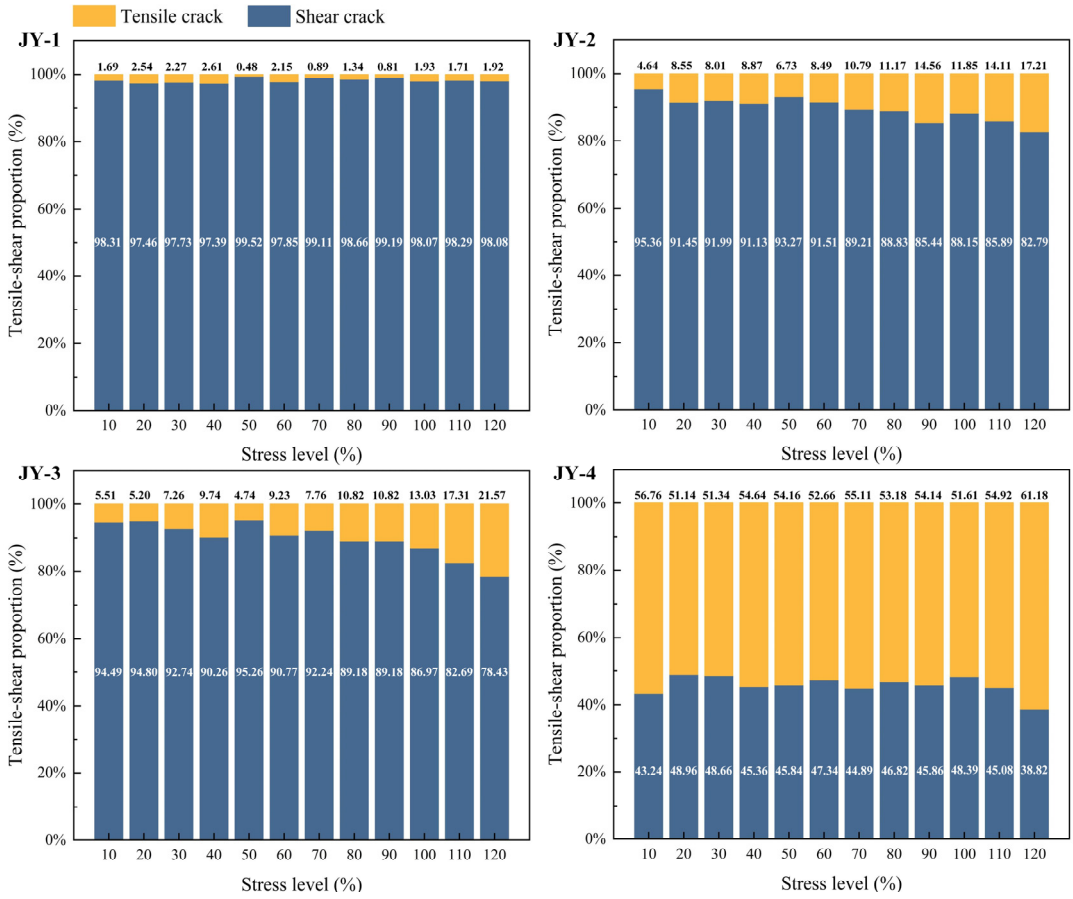

Fig. 10 Fracture mechanism evolution process of rock-like models

Due to the presence of prefabricated fissures, the model exhibits distinct shear failure characteristics. This is manifested by the dominance of shear failure prior to the occurrence of peak stress. For the JY-4 model, this is reflected in a marked increase in the proportion of shear fractures (90%~100% peak stress). It is noteworthy that as the strength decreases, the model becomes more prone to generating a significant number of tensile cracks, with this transition occurring between 50%~90% of the pre-peak stress and the post-peak stage. During this process, small-scale fractures in the model also increase, specifically manifested by the development of the fracture process zone at the tips of surface cracks, which accompanies this transition in fracture mechanisms.

The overall instability process and failure mechanisms of the model are significantly influenced by prefabricated fissures and compressive strength (Su *et al*. 2025a, Wang *et al*. 2023, Xu *et al*. 2024, Kong *et al*. 2021, Farhad *et al*. 2024). Firstly, models with higher compressive strength demonstrate greater capacity for strain energy accumulation, which facilitates more pronounced local deformation development and enables clearer observation of large-scale localized damage. Their failure is more susceptible to fracture influence, exhibiting marked differences between global and local deformation. In contrast, lower-strength models exhibit delayed emergence of high-stress surface areas due to their stress redistribution capabilities. Although local deformation growth rates exceed global deformation after peak stress, they never surpass the overall deformation magnitude.

Furthermore, a key observation in this study is that JY-3 (which possesses lower yield strength but higher elastic modulus than JY-2) demonstrated notably more rapid fracture propagation with distinct brittle failure characteristics. This phenomenon indicates that when models combine low strength with poor deformability, the evolution of the fracture process zone may become excessively rapid and consequently go undetected.

The stronger the overall resistance to model damage, the more likely it is to cause energy accumulation and eventually large-scale damage. Interestingly, the strengths of models JY-2 and JY-3 are similar; however, the elastic modulus of JY-3 is higher, and the local destruction of the JY-3 model dominates the overall instability in a more pronounced manner compared with that of JY-2. This may be due to the fact that the JY-3 model had a higher modulus, and the overall stress of the model increased faster under the same displacement loading rate condition, which exacerbated the stress concentration at the prefabricated fissure while the overall deformation response of the model was relatively slow, which made it too late to dissipate the energy. This ultimately led to a rapid accumulation of energy locally, dominated by a small number of large-scale ruptures and, due to its lower strength compared with the

model JY-2, the stresses required for the destructive effect were low, which is indicative of evident short-term brittle damage characteristics. Under comparable load-bearing capacities, structural specimens with elevated stiffness exhibit greater vulnerability to localized stress concentrations; they demonstrate more pronounced strain localization and typically display more abrupt fracture propagation.

Analysis of acoustic emission RA-AF values indicates that as loading progresses (Fig. 10), the model transitions from shear-dominated crack propagation to an increased occurrence of tensile cracks following peak stress. With decreasing material strength, the proportion of tensile cracks progressively rises, shifting the failure mode from primarily shear-driven to a combined shear-tensile mechanism. This transition is corroborated by the evolution of horizontal displacement patterns observed in Fig. 9.

Comparative studies between manufactured analog materials and natural rock specimens have revealed distinct mechanical behavioral patterns. Gypsum-based specimens typically exhibit pronounced brittle fracture characteristics, yet demonstrate markedly less visible fracture process zone development compared to natural rock formations (Cui *et al*. 2023, Chen *et al*. 2016). Experimental results indicate that specimens possessing simultaneously high elastic modulus and low strength tend to manifest extreme brittle failure modes, with rupture processes occurring too rapidly for effective observation.

This suggests that under identical loading configurations, successful observation of localized fracture mechanisms requires specimens to possess both elevated strength and enhanced elastic modulus. Such mechanical properties induce slower global deformation rates, thereby extending the temporal window available for monitoring the evolution of localized rupture processes. When controlling for identical strength and modulus parameters, increased loading rates of force or displacement (within quasi-static ranges) further influence the temporal development of fracture zones (Li *et al*. 2024b, Wang *et al*. 2018, Wang *et al*. 2024a, Zhao *et al*. 2024). Higher loading conditions generally compress the available observation timeframe, while moderate rates permit more detailed monitoring of progressive failure mechanisms.

Although this study has elucidated the energy release and fracture mechanisms of the model, certain limitations remain. Experimental results demonstrate that the evolution of AE signals can serve as one criterion for evaluating the model's cracking process. DIC analysis reveals that stress concentration induced by prefabricated fissures and deformation localization play decisive roles in model instability. Factors influencing these parameters include fracture length (Wang *et al*. 2025), and the number of prefabricated fissures (Haeri *et al*. 2013). Furthermore, the mineral composition of rocks constitutes a crucial factor affecting their mechanical properties (Zhang *et al*. 2025a). Currently, there is insufficient comparative analysis between rock-like materials and natural rocks regarding mineral composition, as well as limited understanding of the mechanisms through which different mixture components influence mechanical characteristics. Future research should develop formulations that can simulate both the mechanical properties and mineral compositions of natural rocks, thereby providing more reliable references for researchers.

Moreover, given that natural rocks exist in triaxial stress environments (Zheng *et al*. 2023), this study was limited by experimental conditions and could not investigate rock fracture processes under multiaxial loading or multiple stress paths. In recent years, numerous achievements have been made in the quantitative observation of internal strain within models(Su *et al*. 2024, Su *et al*. 2025b), enabling the potential for quantitative assessment of internal deformation energy. Future research should also focus on correlating energy release phenomena inside and outside the models.

5. Conclusions

This study employed four distinct types of rock-similar models. Using AE and DIC techniques, the influence of compressive strength on energy release characteristics and global instability mechanisms was investigated.

(1) During model failure, the process undergoes energy accumulation followed by rapid release, while acoustic emission signals exhibit significant spatiotemporal clustering characteristics. A substantial increase in ring-down counts and AE energy is observed prior to peak stress occurrence.

(2) The fracture mechanism is predominantly governed by prefabricated fissures while being influenced by material strength. Numerous small-scale cracks develop as the model approaches peak stress, accompanied by an increasing proportion of tensile cracks. Local failure at prefabricated fissures precedes global instability, with materials on both sides of fractures demonstrating clear relative sliding tendencies under external loads. Significant local surface deformation can be identified as a precursor to model cracking and instability.

(3) The formulation strength significantly impacts energy storage capacity, AE signals, and surface deformation. High-strength models exhibit relatively fewer fractures with concentrated energy release during post-peak stages. In contrast, low-strength models demonstrate homogeneous energy dissipation with limited energy storage capacity, generating numerous low-energy AE signals. The development of local deformation is affected by the global elastic modulus - when models combine low strength with high modulus, fracture propagation becomes too rapid for effective observation.

Acknowledgements

his work was supported by the National Natural Science Foundation of China (Grant No. 42372322) and the Spark Plan for Earthquake Scienceand Technology (Grant No. XH24060A). The authors would like to thank all the reviewers who participated in the review process as well as MJEditor (www.mjeditor.com) for providing English editing services during the preparation of this manuscript.

References

Aligholi, S., Torabi, A.R., Serati, M. and Masoumi, H. (2024), "The length of fracture process zone deciphers variations of rock tensile strength", *Int. J. Rock Mech. Min. Sci.*, **182**, 105885-105885. https://doi.org/10.1016/J.IJRMMS.2024.105885.

Asemi, F., Lakirouhani, A., Nicksiar, M. and Zohdi, A. (2024), "A new rock brittleness index based on crack initiation and crack damage stress thresholds", *Int. J. Geomech.*, **24**(5). https://doi.org/10.1061/IJGNAI.GMENG-9151.

Cai, W., Zhu, H. and Liang, W. (2022), "Three-dimensional stress rotation and control mechanism of deep tunneling incorporating generalized Zhang–Zhu strength-based forward analysis", *Eng. Geol.*, **308**, 106806. https://doi.org/10.1016/J.ENGGEO.2022.106806.

Chen, F., Du, J., Lv, J., Tang, C. and Pan, Y. (2024a), "Study on the size effect of rock burst tendency of red sandstone under uniaxial compression", *Sci. Rep.*, **14**, 16402. https://doi.org/10.1038/S41598-024-67464-1.

Chen, G., Li, L., Zhao, C. and Huang, R. and Guo, F. (2016), "Acceleration characteristics of a rock slide using the particle image velocimetry technique", *Sensors*, 2650871:1-71:9. https://doi.org/ 10.1155/2016/2650871.

Chen, L., Wang, D., Jiang, Y., Liu, J., Luan, H. and Wu, C. (2024b), "Study on the failure modes of water-bearing soft rock under different low-frequency disturbance", *Eng. Fail. Anal.*, **164**, 108683-108683. https://doi.org/10.1016/J.ENGFAILANAL.2024.108683.

Cheng, T., Wang, L., He, M., Xiao, Y., Li, H. and Wang, T. (2024), "Experimental investigation into grain size effect on failure behavior and nonlinear time-varying acoustic emission series of granite", *Eng. Fail. Anal.*, **162**, 108460. https://doi.org/10.1016/J.ENGFAILANAL.2024.108460.

Cui, X., Wang, J. and Pan, B. (2023), "Comparative analysis of fracture characteristics between rock and rock-like materials", *Heliyon*, **9**, e18486-e18486. https://doi.org/10.1016/J.HELIYON.2023.E18486.

Dong, L., Yang, L. and Chen, Y. (2022), "Acoustic emission location accuracy and spatial evolution characteristics of granite fracture in complex stress conditions", *Rock Mech. Rock Eng.*, **56**, 1113-1130. https://doi.org/10.1007/S00603-022-03124-Y.

Du, K., Luo, X., Liu, M., Liu, X. and Zhou, J. (2024), "Understanding the evolution mechanism and classification criteria of tensile -s hear cracks in rock failure process from acoustic emission (AE) characteristics", *Eng. Fract. Mech.*, **296**, 109864. https://doi.org/10.1016/J.ENGFRACMECH.2024.109864.

Farhadian, H., Tabrizi, D.S., Yousefi, S., Rezaei, A. and Saeidi, A. (2025), "Evaluation of geological hazards along the Karaj water conveyance tunnel using multiple approaches and GIS", *Results in Eng.*, **26**, 104758-104758. https://doi.org/10.1016/J.RINENG.2025.104758.

Guo, R., Zhang, W., Tang, X., Dai, K., Li, Y., Liu, D., Zheng, Y., Zeng, S., Zhou, J. Xu, J. and Sun, H. (2025), "Bridging fault kinematics before, during, and after the 2022 Menyuan earthquake", *Earth Planet. Sci. Lett.*, **666**, 119510-119510. https://doi.org/10.1016/J.EPSL.2025.119510.

Haeri, H., Shahriar, K., Marji, M.F., *et al*. (2012), "Modeling the propagation mechanism of two random micro cracks in rock samples under uniform tensile loading", *Proceedings of the 13th International Conference on Fracture (ICF13)*, China Beijing.

Haeri, H., Shahriar, K., Marji, M.F. and Moarefvand, P. (2014a), "Experimental and numerical study of crack propagation and coalescence in pre-cracked rock-like disks", *Int. J. Rock Mech. Min. Sci.*, **67**, 20-28. https://doi.org/10.1016/j.ijrmms.2014.01.008.

Haeri, H., Shahriar, K., Marji, M.F. and Moarefvand, P. (2014b), "On the strength and crack propagation process of the pre-cracked rock-like specimens under uniaxial compression", *Strength Mater.*, **46**, 140-152. https://doi.org/10.1007/s11223-014-9525-y.

Hu, B., Chen, S., Dan, Y., *et al*. (2025), "Study on the evolution of acoustic signals and strain evolution during large-scale tensile failure test of limestone", *Water Resour. Hydropower Eng. Fail. Anal.*, **56**, 179-193. https://doi.org/10.13928/j.cnki.wrahe.2025.04.015.

Kong, F., Xue, Y., Qiu, D., Li, Z., Chen, Q. and Song, Q. (2021), "Impact of grain size or anisotropy on correlations between rock tensile strength and some rock index properties", *Geomech. Eng.*, **27**(2), 131-150. https://doi.org/10.12989/gae.2021.27.2.131.

Li, K.S., Luan, Y.Q., Yang, S.Q. and Liu, C.X. (2024a), "An experimental investigation on the failure behavior of sandstone with filled fissure under triaxial multilevel cyclic loading", *Fatigue Fract. Eng. Mater. Struct.*, **47**, 3375-3391. https://doi.org/10.1111/FFE.14366.

Li, M., Su, Z., Zang, M., Liu, X., Wang, Y., Wang, Z. and Lu, X. (2024b), "Effect of loading rate on local deformation of rock-like models with locked segment", *J. Mater. Res. Technol.*, **33**, 2868-2878. https://doi.org/ 10.1016/J.JMRT.2024.09.176.

Li, S., Yang, D., Huang, Z., Gu, Q. and Zhao, K. (2022), "Acoustic emission characteristics and failure mode analysis of rock failure under complex stress state", *Theor. Appl. Fract. Mech.*, **122**, 103666. https://doi.org/ 10.1016/J.TAFMEC.2022.103666.

Liu, C., Jiang, Q., Liu, J., Wu, S., Chen, T. and Xiong, X. (2021), "Experimental study on post-peak stick-slip failure of three different rock joints under direct shear tests", *IOP Conference Series: Earth Environ. Sci. Trans.*, 861. https://doi.org/10.1088/1755-1315/861/4/042029

Manouchehrian, A., Sharifzadeh, M., Marji, M.F. and Gholamnejad, J. (2014), "A bonded particle model for analysis of the flaw orientation effect on crack propagation mechanism in brittle materials under compression", *Arch. Civil Mech. Eng.*, **14**, 40-52. https://doi.org/ 10.1016/j.acme.2013.05.008.

Meng, X.X., Yang, S.Q., Song, Y., Zhong, Z., Li, X.S. and Huang, Y.H. (2025), "Study on the true triaxial compression mechanical behavior of fissured granite and its micro-fracture mechanism based on the grain-based model", *Theor. Appl. Fract. Mech.*, **139**, 105051. https://doi.org/10.1016/J.TAFMEC.2025.105051.

Miao, S., Pan, P.Z., Konicek, P., Konicek, P. Yu, P. and Liu, K. (2021), "Rock damage and fracturing induced by high static stress and slightly dynamic disturbance with acoustic emission and digital image correlation techniques", *J. Rock Mech. Geotech. Eng.*, **13**, 1002-1019. https://doi.org/10.1016/J.JRMGE.2021.05.001.

Miao, S., Xia, D., Yang, P., Liu, Z. and Shang, X. (2024), "Characteristics of stress memory and acoustic emission for siltstone under different previous stresses", *Int. J. Geomech.*, **24**(3). https://doi.org/10.1061/IJGNAI.GMENG-8988.

Mostafa, K. and Manoochehr, S. (2018), "Episodic creep events on the San Andreas Fault caused by pore-pressure variations", *Nat. Geosci.*, 610-614. https://doi.org/ 10.1038/s41561-018-0160-2.

Niu, Y., Hu, Y. and Wang, J. (2023a), "Cracking characteristics and damage assessment of filled rocks using acoustic emission technology", *Int. J. Geomech.*, **23**(4). https://doi.org/10.1061/IJGNAI.GMENG-8034.

Niu, Y., Su, Z., Sun, J., Zhang, H., Zhang, M., Wang, L. and Zhang, J. (2023b), "Influence of the strength of rock-like models on the local deformation field and acoustic emission characteristics". *Bull. Eng. Geol. Environ.*, **82**, 334. https://doi.org/10.1007/S10064-023-03355-5.

Ratan, D., Ranbir, D. and Singh, T.N. (2021), "Analysis and prediction of brittle failure in rock blocks having a circular tunnel under uniaxial compression using acoustic emission technique: Laboratory testing and numerical simulation", *Int. J.*

Geo-Eng., 12. https://doi.org/10.1186/S40703-020-00136-X.

Rezvan, A., Mohammad, F.M., Abolfazl, A., *et al*. (2023), "Numerical simulation of fatigue crack propagation in heterogeneous geomaterials under varied loads using displacement discontinuity method", *J. Rock Mech. Geotech. Eng.*, **15**(3), 702-716. https://doi.org/10.1016/J.JRMGE.2022.12.001.

Su, Z., Lu, X., Yin, Q., Tao, Z., Wang, H. and Gan, F. (2025a), "Internal and surface deformation evolution and rupture characteristics of rock-like models with different compression strengths", *Exp. Mech*., 1-20. https://doi.org/10.1007/S11340-025-01236-4.

Su, Z., Niu, Y., Zang, A., Liu, X., Sun, J., Zang, M., Zhou, S., Wang, Z., Li, X. and Zhang, J. (2025b). "Analysis of stresses in gypsum–cement mortar blocks with strike–slip faults of different orientations inferred from acoustic emission and embedded strain sensors", *Rock Mech. Rock Eng.*, **58**, 3889-3908. https://doi.org/ 10.1007/S00603-024-04356-W.

Su, Z., Yoon, J.S., Zang, A., Tang, L., Gu, H. and Zhu, C. (2021), "Stress reorientation by earthquakes near the Ganzi-Yushu strike-slip fault and interpretation with discrete element modelling", *Rock Mech. Rock Eng.*, 1-15. https://doi.org/10.1007/s00603-021-02443-w.

Su, Z., Zhou, S., Zang, A., Sun, J., Zhang, T., Niu, Y., Zhang, J. and Liang, J. (2024), "Analysis of near-field stresses in an analogue strike-slip fault model", *Rock Mech. Rock Eng.*, 1-1. https://doi.org/10.1007/S00603-024-03776-Y.

Wang, L., Hu, X., Wu, N., Zhao, Y., Pang, Y. and Bai, H. (2024a), "Effect of loading rates on mechanical behavior and strain localization characteristics of sandstone", *Environ. Earth Sci.*, **83**, 663-663. https://doi.org/10.1007/S12665-024-11963-X.

Wang, X., Wen, Z., Jiang, Y. and Huang, H. (2018), "Experimental study on mechanical and acoustic emission characteristics of rock-like material under non-uniformly distributed loads", *Rock Mech. Rock Eng.*, **51**, 729-745. https://doi.org/10.1007/s00603-017-1363-3.

Wang, Y., Chen, Z., Yi, X. and Long, D. (2024b), "Macro-meso damage cracking and energy dissipation of rock-backfill composites: Effect of cyclic disturbance frequency", *Fatigue Fract. Eng. Mater. Struct.*, **47**, 2969-2987. https://doi.org/10.1111/FFE.14357.

Wang, Y., Deng, H., Deng, Y., Chen, K. and He, J. (2021), "Study on crack dynamic evolution and damage-fracture mechanism of rock with pre-existing cracks based on acoustic emission location", *J. Petroleum Sci. Eng.*, **201**, 108420. https://doi.org/10.1016/J.PETROL.2021.108420.

Wang, Y., Yi, X., Long, D. and Mao, T. (2023), "On the fracture and energy characteristics of rock–backfill composite structure specimens exposed to fatigue–creep interaction loading", *Fatigue Fract. Eng. Mater. Struct.*, **47**, 153-169. https://doi.org/10.1111/FFE.14175.

Wang, Z., Su, Z., Liu, X., Sun, J., Zang, M., Niu, Y., Zhang, J. and Lu, X. (2025), "Influence of creep–slip fracture length on the local deformation field and fracture characteristics of rock-like models", *Environ. Earth Sci*., **84**, 87-87. https://doi.org/10.1007/S12665-025-12101-X.

Wu, D., Jiang, X., Zhao, Z., *et al*. (2025), "Experimental study on the types and evolution of uniaxial compression cracks in defective sandstone", *Water Resour. Hydropower Eng. Fail. Anal.*, **56**, 200-215. https://doi.org/10.13928/j.cnki.wrahe.2025.02.017.

Wu, H., Ma, D., Spearing, A.J.S. and Zhao, G. (2021), "Fracture response and mechanisms of brittle rock with different numbers of openings under uniaxial loading", *Geomech. Eng*., **25**(6), 481-493. https://doi.org/10.12989/gae.2021.25.6.481.

Wu, X., Zhang, L., Sun, J., Guo, Q., Pan, J. and Gao, J. (2022), "Strength characteristics and failure mechanism of granite with cross cracks at different angles based on dic method", *Adv. Mater. Sci. Eng.*, 2022. https://doi.org/ 10.1155/2022/9144673.

Xu, R., Hu, Y., Yan, Z., Zhao, Y. and Li, Z. (2024), "Experimental investigation on the effect of water saturation on the failure mechanism and acoustic emission characteristics of sandstone", *Int. J. Geomech.*, **24**(6). https://doi.org/10.1061/IJGNAI.GMENG-8526.

Xu, R., Li, Z. and Jin, Y. (2022), "Brittleness effect on acoustic emission characteristics of rocks based on a new brittleness evaluation index", *Int. J. Geomech.*, **22**(10). https://doi.org/10.1061/(ASCE)GM.1943-5622.0002562.

Yang, Z., Zhang, R., Ai, T., Lv, T., Zhang, Z., Xie, J., Li, M., Zhou, J., Zhang, A. and Ren, L. (2024), "Triaxial failure behavior and microfracture source time–frequency characteristics of marble under in situ stress conditions at different depths considering engineering disturbance", *Measurement*, **237**, 115274-115274. https://doi.org/10.1016/J.MEASUREMENT.2024.115274.

Yu, J., Zhang, Q., Zhang, S., Gu, Z. and Jia, C. (2022), "Investigation on fracture mode and initiation mechanisms of cracks in sandstone disk containing a preexisting flaw", *Int. J. Geomech.*, **22**(1). https://doi.org/10.1061/(ASCE)GM.1943-5622.0002231

Zhang, J., Chen, Y., Fang, W., Dong, Y. and Song, Z. (2024), "Acoustic emission and electromagnetic radiation of rock under combined compression-shear loading", *J. Appl. Geophys.*, **226**, 105415. https://doi.org/10.1016/J.JAPPGEO.2024.105415.

Zhang, S., Wang, H., Li, X., Zhang, X., An, D. and Yu, B. (2020), "Experimental study on development characteristics and size effect of rock fracture process zone", *Eng. Fract. Mech*., **241**, 107377. https://doi.org/10.1016/j.engfracmech.2020.107377.

Zhang, S., Xu, Y., Xing, Q., Cui, X., Ji, W. and Li, J. (2025a), "Numerical study on micro-cracking behavior and damage model for granite during thermal-cooling cycles", *Eng. Fract. Mech.*, **329**, 111601. https://doi.org/10.1016/J.ENGFRACMECH.2025.111601.

Zhang, X.P., Liu, Q., Wu, S. and Tang, X. (2015), "Crack coalescence between two non-parallel flaws in rock-like material under uniaxial compression", *Eng. Geol.*, **199**, 74-90. https://doi.org/ 10.1016/j.enggeo.2015.10.007.

Zhang, Y.Y., Xu, W., Zhao, G., Su, K., Chen, Y., Zhao, B., Zhang, Q. and Zhao, J. (2025b), "Mechanical behaviors and energy evolution of sandstone under triaxial cyclic loading", *Environ. Earth Sci*., **84**, 591-591. https://doi.org/10.1007/S12665-025-12587-5.

Zhao, Q., Tu, M., Fu, B., Li, J., Dang, J. and Qi, C. (2024), "Acoustic emission and failure characteristics of coal and rock under single-free-face true triaxial loading", *Eng. Fail. Anal.*, **161**, 108299. https://doi.org/10.1016/J.ENGFAILANAL.2024.108299.

Zheng, Z., Cai, Z., Su, G., Huang, S., Wang, W., Zhang, Q. and Wang, Y. (2023), "A new fractional-order model for time-dependent damage of rock under true triaxial stresses", *Int. J. Damage Mech.*, **32**(1), 50-72. https://doi.org/10.1177/10567895221124325.

Zhou, C., Gao, W., Hu, C., Chen, X. and Cui, S. (2022), "Numerical study of related factors affecting mechanical properties of fractured rock mass and its sensitivity analysis", *Comput. Particle Mech.,* **10**, 369-386. https://doi.org/10.1007/S40571-022-00500-X.

Zhou, X.P. and Zhang, J.Z. (2021), "Damage progression and acoustic emission in brittle failure of granite and sandstone", *Int. J. Rock Mech. Min. Sci.*, **143**, 104789. https://doi.org/10.1016/J.IJRMMS.2021.104789.

Zhu, H., Cai, W. and Liang, W. (2023), "GZZ strength-based three-dimensional analysis theory and stress-controlled design method in deep tunneling", *Chin. J. Rock Mech. Eng.*, **42**, 1-27. https://doi.org/10.13722/j.cnki.jrme.2022.0667.

Zuo, J.P., Li, H.T., Xie, H.P., Ju, Y. and Peng, S. (2007), "A nonlinear strength criterion for rock-like materials based on fracture mechanics", *Int. J. Rock Mech. Min. Sci.*, **45**(4), 594-599. https://doi.org/10.1016/j.ijrmms.2007.05.010.

CC